Materials Science

DOI: 10.1002/anie.201202078

# Microfluidic Control of the Internal Morphology in Nanofiber-Based Macroscopic Cables**

*Daisuke Kiriya, Ryuji Kawano, Hiroaki Onoe, and Shoji Takeuchi**

Assemblies of nanofibers with macroscopic dimensions are utilized in a variety of fields, including the production of electronic and optical sensors[1–3] and scaffolds for living tissues.[4,5] A significant number of nanofiber assemblies are currently being generated using various bioorganic/synthetic nanofibers (e.g., carbon nanotubes (CNTs), DNA molecules, and protein fibrils).[6–10] For integration of nanofibers into materials, macroscopic cables comprising assembled nanofibers have recently attracted much attention.[11–18] These cables are typically produced by microfluidic elongational flow processes, and thus the nanofibers in the cable become oriented along the long axis.[11,15–18] This anisotropic orientation provides a number of potential advantages including improvements in mechanical strength[11,13–16] and directional control of cell growth and chemical synthesis.[15,18] To expand on the advantages of the anisotropic properties of these macroscopic cables, control of the orientation of the nanofibers in a direction other than the long axis is also essential, because the physicochemical properties of assembled structures are strongly dependent on their internal morphology.[19–21] However, because conventional fluidic approaches only focus on using the elongational flow, control of the internal morphology of the macroscopic cables has not been achieved. In this study, we demonstrate control over the internal morphology of macroscopic cables of assembled nanofibers. We employ expansion flow in a coaxial microfluidic channel in addition to the elongational flow. By regulating both elongational and expansion flows at the tip of the micronozzle of the coaxial channels, the nanofibers can be oriented parallel or perpendicular to the channel, respectively (Figure 1). Furthermore, curing of the controlled flow leads to gel cables of nanofiber assemblies with specific (parallel/perpendicular) orientations. These materials with controlled morphology exhibit a remarkable improvement in their electrical conductivity and also mechanical properties that depend on the orientation of the nanofibers. As our study considers only the fluid flow of nanofiber suspensions, this

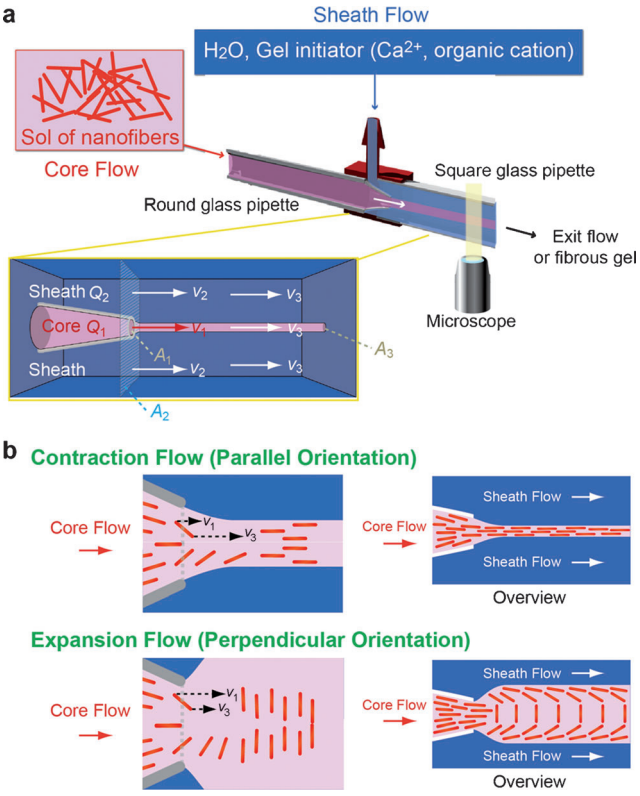


***Figure 1.*** Concept of the microfluidic control of internal morphologies. a) A schematic illustration of the experimental setup. We used a coaxial microfluidic device equipped with two inlets for the core and sheath flows. Nanofiber suspensions are introduced as a core flow ($Q_1$ μL min$^{-1}$, cross-sectional area is $A_1$), and the flow is covered by a sheath flow of deionized (DI) water or gel initiators ($Q_2$ μL min$^{-1}$, cross-sectional area is $A_2$). The combined flows are monitored through a microscope placed downstream. The mean flow velocity of the combined flow and the cross-sectional area of the core flow after combining are labeled $v_3$ and $A_3$, respectively. b) Internal morphologies of the flows in the coaxial microfluidic device. In the contraction flow, i.e., $v_1/v_2 < 1$, the nanofibers are perturbed to orient along the flow stream. In the expansion flow, i.e., $v_1/v_2 > 1$, the nanofibers in the center region are oriented perpendicular to the stream. The overall orientation of the nanofibers shows a parabolic shape that includes perpendicular orientation in the center of the core flow.

[*] Dr. D. Kiriya, Dr. H. Onoe, Prof. Dr. S. Takeuchi
Institute of Industrial Science, The University of Tokyo
4-6-1 Komaba, Meguro-ku, Tokyo (Japan)
and
ERATO Takeuchi Biohybrid Innovation Project, JST
Komaba Open Laboratory (KOL) Room M202
4-6-1 Komaba, Meguro-ku, Tokyo (Japan)
E-mail: takeuchi@iis.u-tokyo.ac.jp
Dr. R. Kawano
Bio Microsystems Project
Kanagawa Academy of Science and Technology (KAST)
Kawasaki City (Japan)

[**] This work was supported by JST (Japan Science and Technology Agency). S. Mori (The University of Tokyo) is thanked for her dedicated help for measuring surface profiles, IR spectroscopy, and SEM observations. We thank A. Sato (The University of Tokyo) for the illustration of the graphical images and S. Iwanaga (The University of Tokyo) and M. Takinoue (Tokyo Institute of Technology) for their helpful discussions. R.K. was financially supported by MEXT.

Supporting information for this article is available on the WWW under http://dx.doi.org/10.1002/anie.201202078.

method is applicable to a variety of anisotropic materials, such as fibers and tubes, and can be used to enhance the resultant physicochemical properties.

We controlled the internal morphology of the nanofiber assemblies by regulating the flow rates of the core and sheath flows in a coaxial microfluidic device. The coaxial microfluidic device was constructed using two glass pipettes. A pulled round glass pipette was inserted into a square glass pipette, which acted as an outlet (Figure 1 and Figure S1 in the Supporting Information).

The core flow of the nanofiber suspension was introduced from a round pipette, such that the suspension jets into the square glass pipette and combines with the sheath flow of aqueous or ionic solutions. The combined flows were observed using a microscope. The relationship between the flow velocities of the core ($v_1$), sheath ($v_2$), and combined flows ($v_3$), the volume flow rates of the core ($Q_1$) and the sheath flows ($Q_2$) are described by the following equation (more details are available in the Supporting Information):

$$v_3 = (Q_1 + Q_2)/(A_1 + A_2) = (A_1 v_1 + A_2 v_2)/(A_1 + A_2), \quad (1)$$

where $A_1$ and $A_2$ denote the cross-sectional area and the outer cross-sectional area of the outlet in the round capillary, respectively. Under laminar flow conditions, the cross-sectional area of the core flow changes to $A_3$ upon combining with the sheath flow. The relationship between $A_1$ and $A_3$ are described in the following manner:

$$A_3 = A_1\ (v_1/v_3). \quad (2)$$

When the velocity of the combined flow is higher than that of the core flow, that is, $v_1 < v_3$, the cross-sectional area of the core flow decreases upon combining with the sheath flow, that is, $A_1 > A_3$; this condition is obtained from Equation (2). More importantly, under these conditions, the contraction flows induce an elongational flow, which allows the nanofibers to be oriented along the flow stream at the tip of the round glass capillary[22] (Figure 1b). This contraction flow is observed when the velocity of the sheath flow is higher than that of the core flow, that is, $v_1/v_2 < 1$, which is governed by the relation obtained from Equation (1). In contrast, when $v_1 > v_3$ [i.e., $v_1/v_2 > 1$ from Eq. (1)], an expansion flow is generated and the cross-sectional area of the core flow increases upon combining with the sheath flow, that is, $A_1 < A_3$. In this situation, the nanofibers are perturbed in the direction perpendicular to the flow at the tip of the round glass capillary (Figure 1b). This situation has been described in former reports[22,23] and it leads to nanofibers that are oriented perpendicular to the flow direction. More precisely, nanofibers are oriented in parabolic shape that includes perpendicular orientation in the center of the core flow and parallel orientation at the interlayer between core and sheath flows (Figure 1b); hereafter this internal morphology is called perpendicular orientation. In summary, we demonstrate the following microfluidic control regime: i) parallel orientation of the nanofibers is achieved using the contracted core flow conditions (contraction flow), wherein $A_1 > A_3$ and $v_1/v_2 < 1$, and ii) the perpendicular orientation is achieved using the expanded core flow conditions (expansion flow, wherein $A_1 < A_3$ and $v_1/v_2 > 1$).

We examined the internal morphology of a nanofiber suspension generated by using variable flow rates. We chose vanadium pentoxide ($V_2O_5$) as the nanofiber material, because the negative charges on the $V_2O_5$ nanofibers stabilize the suspension.[24,25] Figure 2a shows a bright-field image of the flow for the nanofiber suspensions prepared under the contraction flow conditions ($v_1/v_2 = 0.36$ (Table S1 in the Supporting Information); $Q_1 = 20\ \mu L\,min^{-1}$; $Q_2 = 4000\ \mu L\,min^{-1}$) with deionized (DI) water used for the sheath flow. A polarized microscopy image of the same region of the flow shows a bright-yellow line (Figure 2b). This bright-yellow line is due to the birefringence of the flow, which indicates that the nanofibers are oriented parallel to the channel. This parallel orientation was further supported by an image of the microfluidic channel arranged parallel with respect to the polarizers (see Figure S2 in the Supporting Information). A dark image was observed because the direction of the nanofibers is parallel with respect to the polarizers.

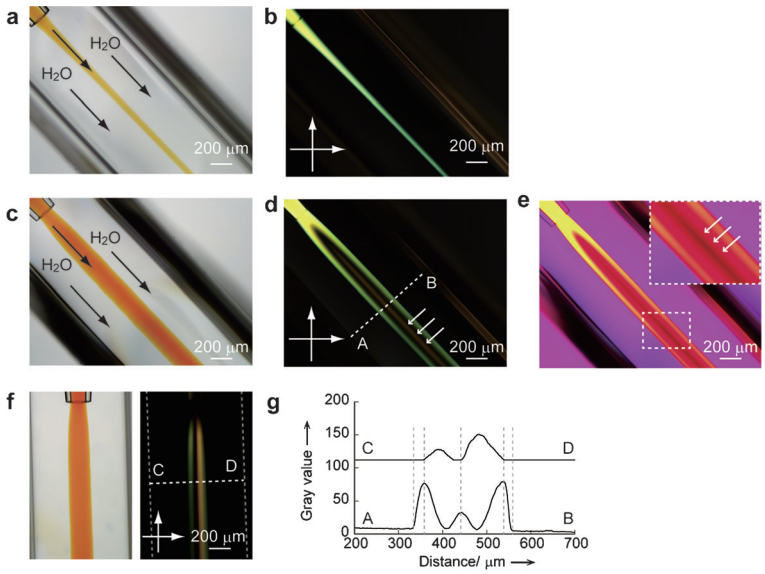


***Figure 2.*** a) Bright-field microscopy image of the $V_2O_5$ nanofiber suspension flow under the contraction flow condition ($Q_1 = 20\ \mu L\,min^{-1}$ and $Q_2 = 4000\ \mu L\,min^{-1}$ in device 1 (see Figure 3a), $v_1/v_2 = 0.36$). The sheath flow consists of DI water. b) A polarized microscopy image of the same region shown in (a). The flows show a parallel orientation. c) Bright-field microscopy image of the $V_2O_5$ nanofiber suspension flow in the expansion flow condition ($Q_1 = 240\ \mu L\,min^{-1}$ and $Q_2 = 4000\ \mu L\,min^{-1}$ in device 1, $v_1/v_2 = 4.3$). d, e) Polarized microscopy image and image resulting from cross-polarizing with a 530 nm retardation plate at the same region shown in (c). The inset in (e) shows an enlarged image of the selected area in (e). f) Bright-field (left) and polarized microscopy (right) images of the expansion flow. The device is arranged in parallel orientation to a polarizer. g) Light intensity (gray value) curve along A—B in (d) and C—D in (f).

Under the expansion flow conditions (i.e., $v_1/v_2 > 1$), the internal morphology of the core flow is visibly different. The bright-field image in Figure 2c demonstrates that the width of the core flow increases after combining with the sheath flow ($v_1/v_2 = 4.3$; $Q_1 = 240\ \mu L\,min^{-1}$; $Q_2 = 4000\ \mu L\,min^{-1}$). A polarized microscopy image of the flow shows two bright lines on the edges and a weak red line in the center (Figure 2d). The edge and center lines were colored yellow and green, respectively, when a 530 nm retardation plate was placed under the cross-polarizers (Figure 2e and Figure S3 in the Supporting Information). These observations indicate a different orientation of the nanofibers at the center than at the edges of the core flow. The microfluidic channel was also placed in a parallel arrangement with respect to the polarizers, which revealed two bright lines separated by a dark line in the center (Figure 2f). The light intensity curves of Figure 2d and f show the overlap between the center regions (Figure 2g). From these results we conclude that the nanofibers were oriented in a parabolic shape that included a perpendicular orientation in the central region of the core flow (Figure 1b).

To examine the transformation of the flows, we monitored the internal morphology of the flow as it was shifted from the contraction to the expansion regime by changing the flow rates in the region of $Q_1 = 20\ \mu L\,min^{-1}$, $Q_2 = 100$–$4000\ \mu L\,min^{-1}$ ($0.36 < v_1/v_2 < 15$) and $Q_1 = 240\ \mu L\,min^{-1}$, $Q_2 = 500$–$4000\ \mu L\,min^{-1}$ ($4.3 < v_1/v_2 < 8.6$). We observed that the internal morphology was gradually transformed from the parallel to the perpendicular orientation as the velocity of sheath flow increased (see Figure S4 in the Supporting Information). Therefore, the internal morphologies of flows were controlled in a stepwise fashion. The key experimental setup was the coaxial flow system, which allowed for accurate and convenient control of the core and sheath flows.

To obtain a macroscopic material with controllable internal morphology, we fabricated macroscopic gel cables by introducing gel initiators to the sheath flow. Macroscopic gel cables were formed using a $V_2O_5$ suspension and a solution of calcium chloride ($CaCl_2$) for the core and sheath flows, respectively; $V_2O_5$ suspensions form gels in the presence of cations (Figure 3a). By using two types of devices (devices 1 and 2), we formed cables with widths that varied from 40 to 690 μm (Figure 3b–d and Table S2 in the Supporting Information); in devices 1 and 2, the inner diameters of the tips of the round glass pipettes were 130 and 600 μm, respectively. Scanning electron microscopy (SEM) indicated that the dried gel cables were composed of very thin flattened structures with a high aspect ratio (Figure 3e,f and Figure S5 in the Supporting Information). The mean thickness of the cables, determined using a surface profiler, was found to be several hundred nanometers (Figure 3g and Table S2 in the Supporting Information). An appreciable difference was observed in the thicknesses of the cables fabricated using devices 1 and 2 at the same flow rate ($Q_1 = 240\ \mu L\ min^{-1}$ and $Q_2 = 4000\ \mu L\,min^{-1}$). In general, the dimensions (radii, widths, and thicknesses) of the core flow depended on the volume flow rates ($Q_1$ and $Q_2$) and not on the inner diameters of the tips of the round glass pipettes in the device[26,27] (see Figure S2 in the Supporting Information). In this context,

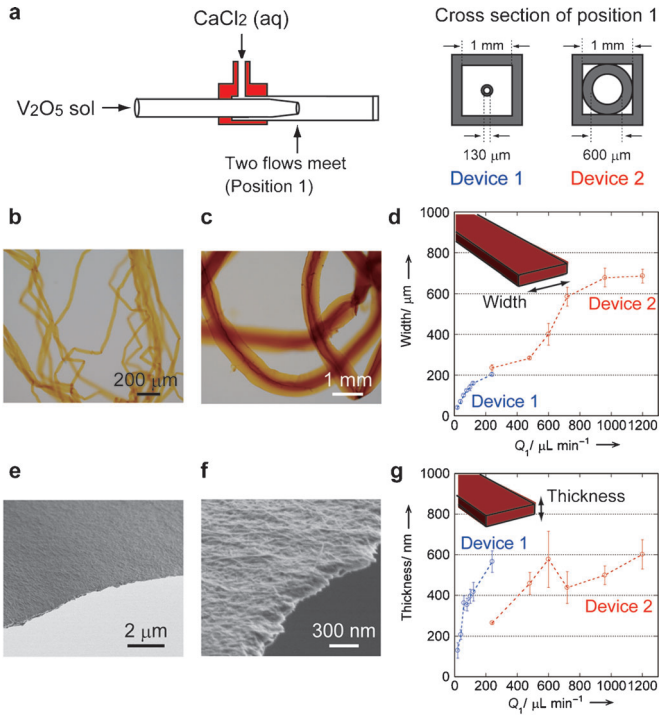


***Figure 3.*** a) Illustration of the coaxial microfluidic device. $V_2O_5$ suspension and $CaCl_2$ (gel initiator) solution are introduced as core and sheath flows, respectively. Device 1 and device 2 have inner diameters of 130 and 600 μm, respectively. b) Bright-field images of the gel cables obtained for the condition of $Q_1 = 20\ \mu L\,min^{-1}$ for device 1 and c) $Q_1 = 1200\ \mu L\,min^{-1}$ for device 2, where $Q_2$ is $4000\ \mu L\,min^{-1}$. d) $Q_1$-dependent widths of the dried cables. The cables are fabricated with variable conditions of $Q_1$, where $Q_2$ is $4000\ \mu L\,min^{-1}$. e,f) Flat shape of the dried gel cable observed using SEM ($Q_1 = 20\ \mu L\,min^{-1}$ and $Q_2 = 4000\ \mu L\,min^{-1}$ for device 1). g) Plots of the thicknesses of dried gel cables against the core flow rate ($Q_1$). All sheath volume flow rates are $4000\ \mu L\,min^{-1}$

we postulated that the difference in the thickness of the two cables arises from the difference in the internal morphologies of the gel cables, because the cables were fabricated using different velocity conditions: contraction ($v_1/v_2 < 1$) flow in device 2 and expansion ($v_1/v_2 > 1$) flow in device 1 (see below).

In fact, the difference in the internal morphology was revealed using a polarized microscope. Figure 4a shows the gel cable that was fabricated using device 2 under the contraction flow condition ($v_1/v_2 = 0.046$; $Q_1 = 240\ \mu L\,min^{-1}$ and $Q_2 = 4000\ \mu L\,min^{-1}$). The wide yellow line indicates that the $V_2O_5$ nanofibers were strongly oriented parallel to the long axis of the cable. The brightness curve also indicates that the samples exhibited a uniform birefringence. A dark image was observed when the cables were arranged parallel with respect to the orientation of the polarizers (see Figure S6 in the Supporting Information). In contrast, the gel cable obtained using device 1 under the same flow rates ($Q_1 = 240\ \mu L\,min^{-1}$ and $Q_2 = 4000\ \mu L\,min^{-1}$) showed a completely different internal morphology that was attributed to the use of an expansion flow condition ($v_1/v_2 = 4.3$, Figure 4b). The brightness curve shows the same trend that is observed in the nanofiber suspension flow under the expansion flow condi-

  

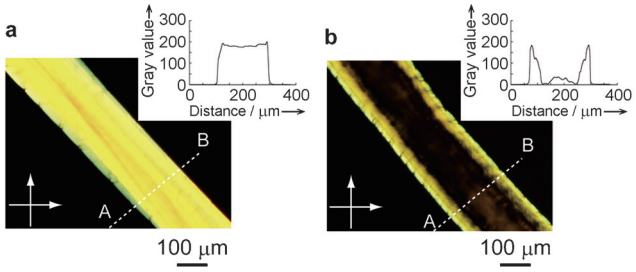


***Figure 4.*** Polarized microscopy images of the $V_2O_5$ gel cables and the brightness intensity (gray value) profiles along A–B lines in each image. a, b) The gel cables fabricated using the condition of $Q_1 = 240\ \mu L\ min^{-1}$, $Q_2 = 4000\ \mu L\ min^{-1}$ for device 2 ($\nu_1/\nu_2 = 0.046$, (a)) and device 1 ($\nu_1/\nu_2 = 4.3$, (b)). Inserted profiles indicate the parallel and perpendicular orientations of nanofibers in (a) and (b), respectively. The crossed arrows in images indicate the direction of polarizers.

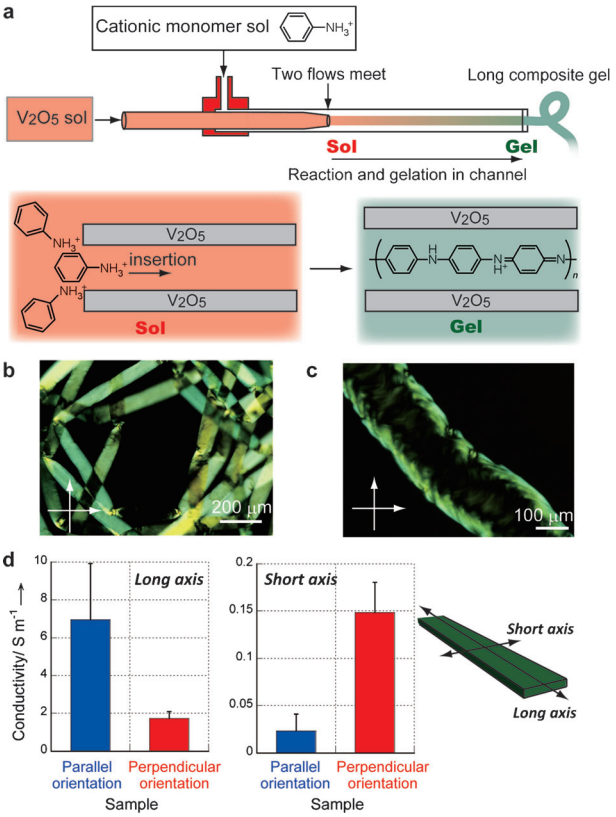


***Figure 5.*** Template synthesis for organic/inorganic hybrid gel cables with specific anisotropic properties. a) Illustration of the fabrication process of organic/inorganic hybrid gel cables in microfluidic channels. A $V_2O_5$ suspension and a cationic monomer (anilinium ion) solution are introduced as core and sheath flows, respectively. Anilinium cations induce the gelation of $V_2O_5$. Simultaneously, anilinium cations are inserted into $V_2O_5$ nanoslits and polymerized into polyaniline by a redox reaction with $V_2O_5$. b, c) Polarized microscopy images of polyaniline/$V_2O_5$ composite gels obtained for the conditions $Q_1 = 40$ ($\nu_1/\nu_2 = 0.71$, (b)) and $240\ \mu L\ min^{-1}$ ($\nu_1/\nu_2 = 4.3$, (c)), while the other conditions ($Q_2 = 4000\ \mu L\ min^{-1}$ for device 1) are the same. d) Conductivities along the long and short axes of the cables (assignments are shown in the image) with the parallel (shown in (b)) and perpendicular orientations (shown in (c)) of nanofibers. The results are shown as the mean ± standard error of the mean ($N = 3$). The crossed arrows in images (b) and (c) indicate the direction of polarizers.

tion (Figure 2d). The data indicated that the gel cable consisted of a perpendicular orientation of the nanofiber assemblies. The perpendicular orientation is further supported by the images that were obtained using cross-polarizers that contained a 530 nm retardation plate; in these images the edges of the gel cable have a different color than the center of the gel cable (Figure S7 in the Supporting Information). Therefore, we fabricated two types of gel cables with different internal morphologies (parallel and perpendicular orientations) by controlling the velocity of the flow using devices 1 and 2. The above phenomena can also be reproduced using a single device and only changing either the core or sheath flow rate, which induces a transformation of the internal morphology (Figure S8 in the Supporting Information). In this manner, we have shown that a coaxial microfluidic device can be used to obtain solidified phases with controlled internal morphologies that are consistent with the flow morphologies in the device as shown in Figure 2.

To apply our approach to the production of functional materials, we examined the fabrication of two composite gel cables: 1) composite cables composed of a conductive organic polymer and $V_2O_5$ nanofibers, which were fabricated using a template synthesis within the microfluidic channel; and 2) a polysaccharide gel that confined carbon nanotubes (CNTs) with the controlled orientation.

To produce conductive polymer/$V_2O_5$ composite cables, we utilized the redox activity of $V_2O_5$ (Figure 5a). We introduced an anilinium chloride solution into the microfluidic channel as the sheath flow. Anilinium ions are polymerized into a conductive organic polymer (polyaniline) when they undergo a redox reaction with $V_2O_5$.[28,29] This polymerization reaction allows the anilinium ions to be incorporated into the nanoslits of the $V_2O_5$ nanofibers and react at the vanadium sites. Simultaneously, the gelation of $V_2O_5$ suspension is induced by the presence of cationic anilinium ions. Figure 5b shows a composite polyaniline/$V_2O_5$ gel cable that was fabricated under a contraction flow condition ($\nu_1/\nu_2 = 0.71$) using device 1 (see Figures S9 and S10 in the Supporting Information for identifying the cables). The nanofibers appear to be oriented parallel to the long axis of the cable, as shown in Figure 4a (see Figure S11 in the Supporting Information for further information). In contrast, the perpendicular orientation is observed when the composite gel is fabricated using the expansion flow condition ($\nu_1/\nu_2 = 4.3$, Figure 5c and Figure S11 in the Supporting Information); the internal morphology is the same as that shown in Figure 4b. Interestingly, the conductivity is strongly dependent on the internal morphology of the cables. We analyzed the conductivity along the long and short axes of the cables. The cable with a parallel orientation of the nanofibers (shown in Figure 5b) exhibits a 300-fold higher conductivity along the long axis than along the short axis (Figure 5d and Table S3 and Figure S12 in the Supporting Information). In contrast, for the perpendicular orientation of the nanofibers shown in Figure 5c, the conductivity anisotropy exhibits only an 11-fold

  

difference for the long and short axes of the cables (Figure 5d and Table S3 and Figure S13 in the Supporting Information). Therefore, our method enables us to fabricate composite gel cables in a microfluidic channel with a controlled conductivity anisotropy using the same components.

Next, to examine the confinement of functional nanofibers in an oriented manner, we fabricated a polysaccharide gel cable that contained CNTs. For the core flow we used a solution of a common polysaccharide (sodium alginate) and a suspension of CNTs, while a solution of $CaCl_2$ served as the sheath flow; sodium alginate forms gels in the presence of calcium ions.[30] The morphology control (parallel and perpendicular orientations) of the CNTs is indicated using the contraction and expansion flow conditions, respectively (Figure S14 in the Supporting Information). The Young's modulus of the dried cable produced by the contraction flow (1.1 GPa) is greater than that of the cable produced by the expansion flow (0.70 GPa; see Figure S15 in the Supporting Information). Therefore, the flexibility of the gel cable is highly dependent on its internal morphology. The composite gel cables are sufficiently strong to be wounded up over several meters (about four meters); the cables can therefore be easily aligned on the macroscopic scale, even in the case of materials with a lower Young's modulus (Figure S14c–e in the Supporting Information). This mechanical strength is useful for integrating the cables with other materials or devices. Furthermore, the conductivity of each cable along the long axis is also highly dependent on the internal morphology of the cable. The cable with a perpendicular orientation produced under the expansion flow condition exhibited a higher conductivity ($(236 \pm 18)\ S\,m^{-1}$) than the cable produced under the contraction flow condition ($(63 \pm 9)\ S\,m^{-1}$, Figure S14f in the Supporting Information). This result is important when CNTs are used in the matrix, because the CNT nanofibers would connect with one another more effectively when they are in the perpendicular orientation than in the parallel orientation. In a former work, the blending of CNTs into polymer matrices showed shear-induced decrease of conductivity;[31] in our case a similar phenomenon was observed, which might be due to the fact that each CNT should be separated from other CNTs in the parallel orientation in the cable. As shown herein, the proposed method for controlling the internal morphology affords the confinement of the nanofibers with a specific orientation, which significantly influences the resultant physical properties.

We have demonstrated that changes to the internal morphology of nanofiber assemblies from a parallel to a perpendicular orientation are possible using a microfluidic device. The morphology of the nanofibers was found to be highly dependent on the core and sheath flow velocities. This coaxial flow system would be useful to produce a variety of nanofiber-based materials that can exhibit the orientation-driven physical properties such as ferromagnetic/ferroelectric properties and optical anisotropy. This study is also expected to contribute to the design of scaffolds for tissue engineering, because the proliferation of cells is known to be highly dependent on the morphology of the scaffolds.[32] Thus, our approach should have an impact on structure-derived functional materials based on nanofiber assemblies.

Received: March 15, 2012
Revised: June 26, 2012
Published online: July 23, 2012

**Keywords:** gels · microfluidics · nanofibers · organic–inorganic hybrid composites

[1] Z. Y. Fan, J. C. Ho, T. Takahashi, R. Yerushalmi, K. Takei, A. C. Ford, Y. L. Chueh, A. Javey, *Adv. Mater.* **2009**, *21*, 3730–3743.
[2] M. C. McAlpine, H. Ahmad, D. W. Wang, J. R. Heath, *Nat. Mater.* **2007**, *6*, 379–384.
[3] S. Xu, Z. L. Wang, *Nano Res.* **2011**, *4*, 1013–1098.
[4] C. P. Barnes, S. A. Sell, E. E. D. Boland, D. G. Simpson, G. L. Bowlin, *Adv. Drug Delivery Rev.* **2007**, *59*, 1413–1433.
[5] R. M. Capito, H. S. Azevedo, Y. S. Velichko, A. Mata, S. I. Stupp, *Science* **2008**, *319*, 1812–1816.
[6] M. Zhang, S. Fang, A. A. Zakhidov, S. B. Lee, A. E. Aliev, C. D. Williams, K. R. Atkinson, R. H. Baughman, *Science* **2005**, *309*, 1215–1219.
[7] N. R. Chiou, C. M. Lui, J. J. Guan, L. J. Lee, A. J. Epstein, *Nat. Nanotechnol.* **2007**, *2*, 354–357.
[8] J. Zheng, J. J. Birktoft, Y. Chen, T. Wang, R. Sha, P. E. Constantinou, S. L. Ginell, C. Mao, N. C. Seeman, *Nature* **2009**, *461*, 74–77.
[9] T. P. J. Knowles, T. W. Oppenheim, A. K. Buell, D. Y. Chirgadze, M. E. Welland, *Nat. Nanotechnol.* **2010**, *5*, 204–207.
[10] S. G. Zhang, *Nat. Biotechnol.* **2003**, *21*, 1171–1178.
[11] B. Vigolo, A. Penicaud, C. Coulon, C. Sauder, R. Pailler, C. Journet, P. Bernier, P. Poulin, *Science* **2000**, *290*, 1331–1334.
[12] M. Yaman, T. Khudiyev, E. Ozgur, M. Kanik, O. Aktas, E. O. Ozgur, H. Deniz, E. Korkut, M. Bayindir, *Nat. Mater.* **2011**, *10*, 494–501.
[13] H. W. Zhu, C. L. Xu, D. H. Wu, B. Q. Wei, R. Vajtai, P. M. Ajayan, *Science* **2002**, *296*, 884–886.
[14] Y. L. Li, I. A. Kinloch, A. H. Windle, *Science* **2004**, *304*, 276–278.
[15] S. M. Zhang, M. A. Greenfield, A. Mata, L. C. Palmer, R. Bitton, J. R. Mantei, C. Aparicio, M. O. Cruz, S. I. Stupp, *Nat. Mater.* **2010**, *9*, 594–601.
[16] V. A. Davis, et al., *Nat. Nanotechnol.* **2009**, *4*, 830–834. See the Supporting Information for the complete author list.
[17] L. Biette, F. Carn, M. Maugey, M. F. Achard, J. Maquet, N. Steunou, T. Livage, H. Serier, R. Backov, *Adv. Mater.* **2005**, *17*, 2970–2974.
[18] D. Kiriya, M. Ikeda, H. Onoe, M. Takinoue, H. Komatsu, Y. Shimoyama, I. Hamachi, S. Takeuchi, *Angew. Chem.* **2011**, *124*, 1585–1589; *Angew. Chem. Int. Ed.* **2011**, *51*, 1553–1557.
[19] Y. N. Xia, B. Gates, Y. D. Yin, Y. Lu, *Adv. Mater.* **2000**, *12*, 693–713.
[20] H. Kim, J. Ge, J. Kim, S. Choi, H. Lee, H. Lee, W. Park, Y. Yin, S. Kwon, *Nat. Photonics* **2009**, *3*, 534–540.
[21] S. B. Kharchenko, J. F. Douglas, J. Obrzut, E. A. Grulke, K. B. Migler, *Nat. Mater.* **2004**, *3*, 564–568.
[22] T. Yamamoto, Y. Yamasaki, Y. Tanaka, N. Mori, *J. Cent. South Univ. Technol.* **2007**, *14*, 59–62.
[23] W. J. Choi, S. C. Kim, *Polymer* **2004**, *45*, 2393–2401.
[24] O. Pelletier, P. Davidson, C. Bourgaux, J. Livage, *Prog. Colloid Polym. Sci.* **1999**, *112*, 121–125.
[25] G. Gu, M. Schmid, P. W. Chiu, A. Minett, J. Fraysse, G. T. Kim, S. Roth, M. Kozlov, E. Munoz, R. H. Baughman, *Nat. Mater.* **2003**, *2*, 316–319.
[26] F. Zarrin, N. J. Dovichi, *Anal. Chem.* **1985**, *57*, 2690–2692.

  

[27] W. Jeong, J. Kim, S. Kim, S. Lee, G. Mensing, D. J. Beebe, *Lab Chip* **2004**, *4*, 576 – 580.
[28] M. G. Kanatzidis, C. G. Wu, H. O. Marcy, C. R. Kannewurf, *J. Am. Chem. Soc.* **1989**, *111*, 4139 – 4141.
[29] J. Livage, *Chem. Mater.* **1991**, *3*, 578 – 593.
[30] C. K. Kuo, P. X. Ma, *Biomaterials* **2001**, *22*, 511 – 521.
[31] a) A. E. Eken, E. J. Tozzi, D. J. Klingenberg, W. Bauhofer, *Polymer* **2011**, *52*, 5178 – 5185; b) F. Du, J. E. Fischer, K. I. Winey, *Phys. Rev. B* **2005**, *72*, 121404.
[32] D. Kai, M. P. Prabhakaran, G. R. Jin, S. Ramakrishna, *J. Biomed. Mater. Res. B* **2011**, *98B*, 379 – 386.

  